RSC Advances

PAPER

View Article Online
View Journal | View Issue

Cite this: *RSC Adv.*, 2022, **12**, 9424

Facile preparation of a polypyrrole modified Chinese yam peel-based adsorbent: characterization, performance, and application in removal of Congo red dye†

Yan Wang, * Rongyao Chen, Zijing Dai, Qingcai Yu, Yongmei Miao and Ronghua Xu

In this study, Chinese yam peel (CYP) was modified with polypyrrole *via* an *in situ* polymerization method to remove Congo red from aqueous media. The prepared CYP–polypyrrole (CYP–PPy) composite was characterized using FTIR, SEM, TEM, XRD, TG and BET analysis. The performance of CYP–PPy towards the adsorption of Congo red (CR) was explored in batch mode. The removal efficiency of CR was found to be 86% at the initial concentration of 100 mg L^{-1}, contact time of 120 min, and the adsorbent dosage of 10 g L^{-1}. At equilibrium time (20 h), the removal efficiency was significantly acceptable (98.9%). The adsorption kinetics data were most consistent with the pseudo-second-order kinetic model. The adsorption equilibrium data could be described well by the Langmuir isotherm model with the maximum adsorption capacity of 86.66 mg g^{-1}. In view of thermodynamics, the adsorption process was endothermic and more favorable for CR removal at 45 °C. A reusability study indicated that CYP–PPy could be reused effectively for up to three successive cycles of ad-/de-sorption. Hence, this work provides an alternative scheme for the targeted exploitation of agricultural waste to control dye pollution.

Received 11th November 2021
Accepted 21st March 2022

DOI: 10.1039/d1ra08280a

rsc.li/rsc-advances

1. Introduction

In the last decades, the discharge of significant raw sewage has been the main environmental issue due to the development of industrialization and increasing world population.[1] Therefore, water pollution causes a serious challenge for the global ecosystem.[2] Water is contaminated by various pollutants such as dyes, pharmaceuticals, pesticides, and heavy metals. Among these various destructive contaminants, dyes resulting from textile industries have been considered as the most hazardous, imparting harmful threats on human health and the ecosystem.[3] This is due to their noxious, mutagenic and low-degradable properties. Thus, it is crucial to minimize or remove the dyes before discharging into the water bodies. In this context, many available methods for the treatment and disposal of dyes have been studied, such as adsorption, photocatalytic degradation, chemical precipitation, electrodialysis, and biological treatment.[4–11] In general, each technique has its inherent advantages and disadvantages. Among them, adsorption has been considered as an efficient, economically inexpensive, versatile and eco-friendly process becoming a predominantly-used technique to remove dyes from wastewater. For example, Purkait *et al.* have selected activated carbon as adsorbent for the removal of Congo red.[12] Normally, the removal performance of dyes is strongly reliant on the adsorbent features like porosity, specific surface area, the exposed degree of functional groups, *etc.* Consequently, numerous researchers have made great efforts to produce inexpensive, versatile and effective adsorbing materials for the removal of dyes.

Recently, numerous inorganic and organic based adsorbents have received much attention for the cancellation of contaminants from wastewater. Since the advent of polymer-based adsorbents, conducting polymers have progressively engrossed scholar' considerable attention due to their satisfactory features such as facile synthesis, high stability, non-toxicity, good biocompatibility, low-cost.[3,13–15] Among these polymers, polypyrrole (PPy) has been widely used in environmental studies. Moreover, the PPy has positively charged nitrogen atoms in their structures, being able to remove anionic contaminants from aqueous solution through ion-exchange, electrostatic and π–π interaction.[16–18] Although extensive interest and increasing applications of PPy, the tendency of self-aggregation, poor processability, difficulty in porosity control, and relatively low adsorption capacity are still the main limited-factors in the removal of contaminants from water.[11,19] Accordingly, the preparation of PPy based or modified composites can overcome the main limitations, and be considered as a promising way to improve its performance.[20]

College of Life and Health Sciences, Anhui Science and Technology University, Fengyang 233100, China. E-mail: yanwang0129@126.com

† Electronic supplementary information (ESI) available. See DOI: 10.1039/d1ra08280a

Mashkoor *et al.* integrated polypyrrole with chitosan-based magsorbent for the elimination of methyl orange and crystal violet dyes from aqueous medium.[3] Kamal *et al.* synthesized a ternary nanocomposite comprising the graphene oxide, chitosan, and polypyrrole to remove the Congo red and heavy metals.[21] Hence, polypyrrole based polymeric composites have received much attention and applications in recent years.

Agricultural peels are rich in active functional groups, becoming the promising source of adsorption materials. These wastes have been employed either as biocomposites or natural biosorbents in the removal of contaminants from water.[22,23] For example, Huang *et al.* synthesized a magnetic carbon material based on pomelo peel to extract the pollutants in water environment.[24] It is obvious that agricultural peels serve as an interesting alternative in the low-cost and ecofriendly treatment of contaminants. Yam (*Dioscoreae rhizoma*) is a tuber distributed in tropical and subtropical regions.[25] Chinese yam (CY) serves as the potential functional food, which has been widely used in China. Meanwhile, Chinese yam peel (CYP) is the generation as solid waste lacking further application. Hence, it is meaningful to explore the potential utilization value of CYP.

In this work, we used *in situ* polymerization method to fabricated a Chinese yam peel–PPy composite (CYP–PPy) with satisfactory adsorption efficiency for removal of Congo red (CR) dye from aqueous media. Facile preparation, low-cost, promising adsorption performance, non-toxicity, and enjoying the benefit of PPy are the notable features of CYP–PPy composites. The prepared CYP–PPy composite was characterized with FTIR, SEM, TEM, XRD, TG and BET in detail. Moreover, based on the characterization, a possible adsorption mechanism of CR on CYP–PPy composite was proposed. Batch adsorption experiments were carried out to reveal the kinetic and isotherm process. Finally, the reusability of adsorbent has also been discussed. Herein, Chinese yam peel, as a waste material, can be utilized to produce agricultural waste/polymer composite to provide a reasonable scheme for dye pollution control.

2. Experimental

2.1 Reagents and materials

Pyrrole, Pluronic F127, $FeCl_3$, and Congo red were purchased from Aladdin (China). Chinese yam peel was supplied by a local market. And the other required reagents were purchased from Macklin (China).

2.2 Instrumentation

FTIR spectra were recorded on a spectrometer (PerkinElmer, L1600300, USA) with KBr pellets. SEM (JEOL, JSM-6700F, Japan) was used to capture the surface structure of the adsorbent. TEM (JEOL, JEM-2100F, Japan) was employed to observe the shape and particle size of CYP–PPy composite. XRD (Tokyo, Rigaku, Japan) was used to scrutinize the crystallinity of the material. The thermal stability was characterized by TG analyzer (SDT650, USA) in the temperature range of 30–800 °C in nitrogen atmosphere. The characteristics of adsorbent including surface area, pore volume, and pore diameter were measured *via* BET (Quantachrome, Autosorb iQ, USA). The concentration of CR solution was monitored *via* a UV-visible spectroscopy (DR6000, China).

2.3 Preparation of CYP–PPy composite

The dried CYP powder was soaked in 25 mL aqueous solution of pyrrole (0.2 M) for 20 h. In a separate container, certain amount of Pluronic F127 as dispersant (controlling the shapes and dispersion of PPy) was dissolved in 50 mL deionized water under ultrasound and then 2.03 g $FeCl_3$ as the oxidizing agent was added to the solution, stirred well on a magnetic stirrer to form a homogeneous solution. The resulting solution was poured into the first vessel followed by further stirring at 5 °C for 5 h. The synthesized black CYP–PPy composite was filtered and washed repetitively with deionized water and ethanol. Finally, the resulting composites were dried under vacuum for 24 h and used in removal experiments.

2.4 Adsorption study

The adsorption capacity of composites was investigated for CR removal at different process variables, *i.e.* adsorbent dosage, dye concentration, contact time and temperature. The batch experiments were performed in 50 mL Erlenmeyer flask. A specific amount of composites was mixed with CR solution (25 mL), and the adsorption took place in a shaker incubator at 150 rpm at a scheduled temperature for specific time. The concentration of CR was monitored at the wavelength of 492 nm by UV-visible spectroscopy, and the calibration curve was given in Fig. S1.† Finally, the adsorption capacity was calculated *via* the following equations:

$$q_e = \frac{(C_0 - C_e) \times V}{m} \quad (1)$$

$$q_t = \frac{(C_0 - C_t) \times V}{m} \quad (2)$$

The removal efficiency (E) was evaluated as:

$$E(\%) = \frac{C_0 - C_t}{C_0} \times 100 \quad (3)$$

where q_e and q_t (mg g^{-1}) represent the adsorption capacity at equilibrium and any time, respectively. C_0, C_e and C_t (mg L^{-1}) are the initial, equilibrium and any time concentration, respectively. V (L) and m (g) correspond to the volume of dye solution and the mass of the adsorbent, respectively.

2.5 Desorption and regeneration of the adsorbent

To evaluate the recovery adsorption efficiency of the adsorbent, the adsorbent regeneration tests were conducted with different desorbing solvents, namely, 0.1 M HCl, 0.1 M NaOH and ethanol. After then, the dye-loaded-CYP–PPy adsorbent was rinsed with distilled water to eliminate any excess of desorbing solvent, and then dried under vacuum at 40 °C. The CR concentration applied for each usage cycle was 100 mg L^{-1}. Same procedure was repeated in each adsorption–desorption cycle to re-evaluate the adsorption efficiency of the adsorbent.

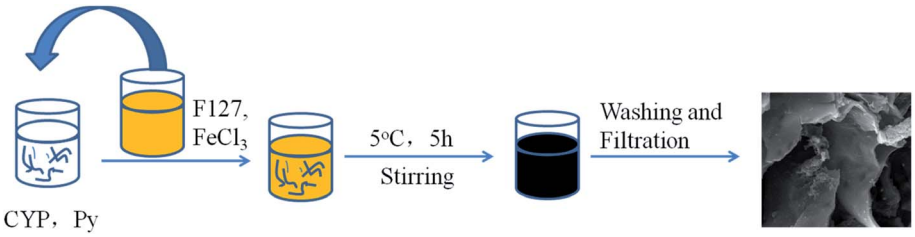

Scheme 1 Schematic illustration of preparation procedure of CYP–PPy composite.

3. Results and discussion

3.1 Synthesis and characterization of CYP–PPy composite

Scheme 1 illustrates the preparation procedure of CYP–PPy composite. CYP is a biomass having active functional groups which can provide active-sites for the polypyrrole on CYP. Adding the $FeCl_3$ solution as the oxidizing agent generates oxidative polymerization. The prepared CYP–PPy composite was characterized using different techniques.

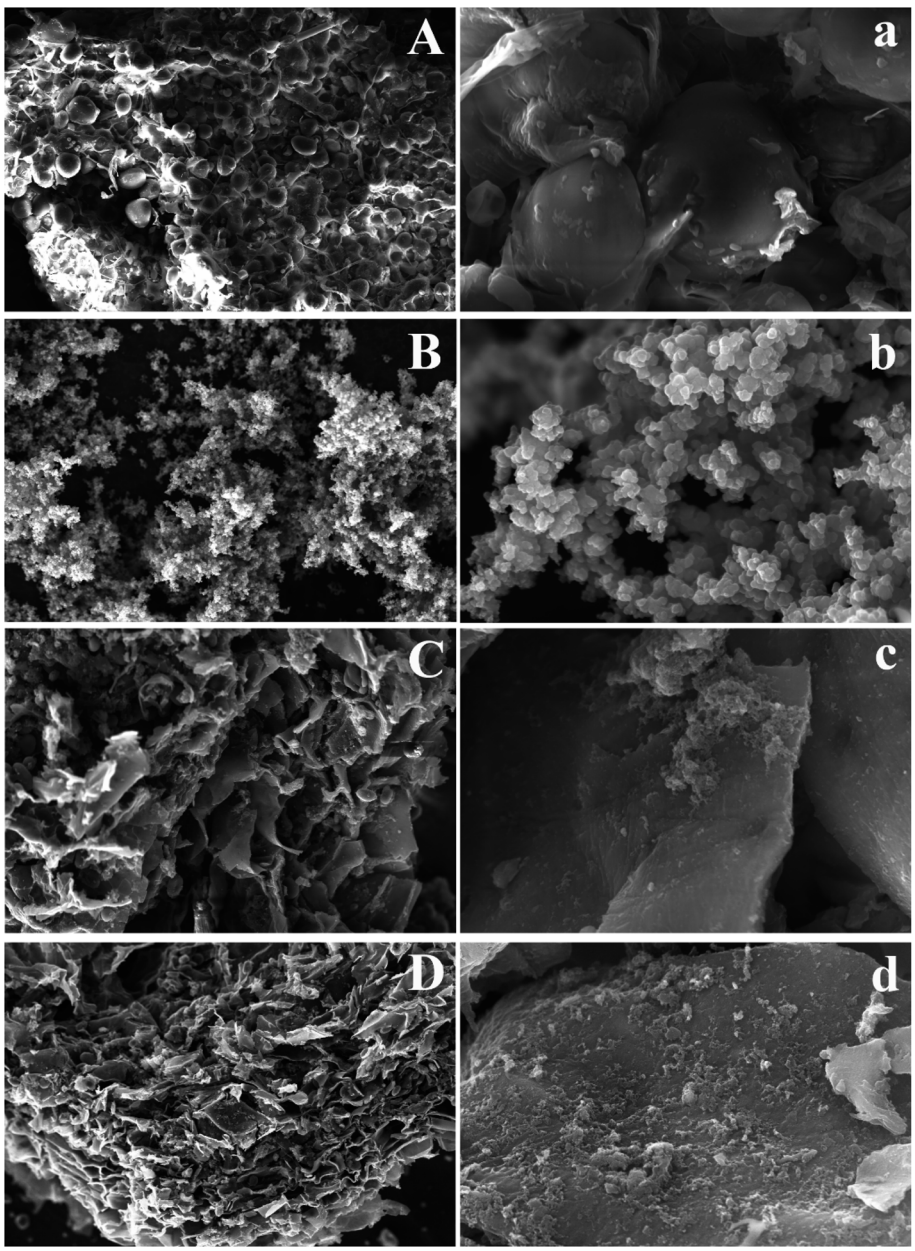

Fig. 1 SEM images of CYP (A(a)), PPy (B(b)), CYP–PPy (C(c)), and CR loaded CYP–PPy (D(d)).

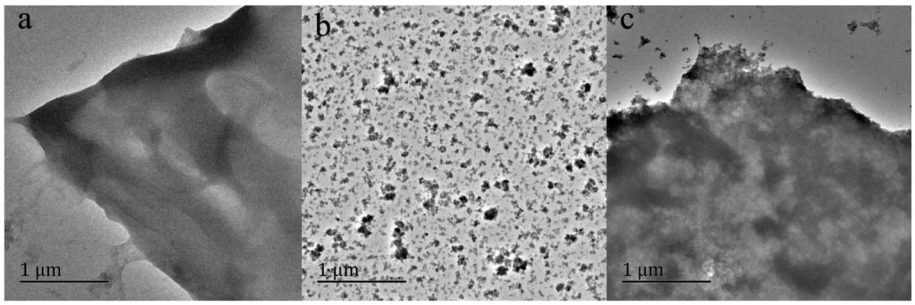

Fig. 2 TEM images of CYP (a), PPy (b) and CYP–PPy (c).

The surface morphologies and structure of CYP, PPy, CYP–PPy, and CR loaded CYP–PPy were observed *via* SEM and the images were illustrated in Fig. 1. The SEM images of CYP (Fig. 1A(a)), having oval or spherical granules morphology, indicate that the starch is existed on the surface of CYP with no distinct cavity at the edge of the fold. The pure PPy powder (Fig. 1B(b)) displays as aggregates morphology exhibiting quasi-spherical particles. On the other hand, the CYP is generally coated by PPy during the preparation of CYP–PPy (Fig. 1C(c)). Its surface becomes very rough. After CR adsorption, the surface morphology of CYP–PPy remains nearly unchanged except for a larger dense layer, since the surface of CYP–PPy is covered by the dye (Fig. 1D(d)). The TEM images of CYP, PPy and CYP–PPy composite were displayed in Fig. 2. It was observed that the morphology of CYP was changed after modification with polypyrrole. The image of CYP–PPy suggests that dark patches of PPy particles with diffused morphology dispersed in the CYP matrix.

To verify whether CYP and PPy were successfully binding, FTIR was carried out. Fig. 3a illustrates the FTIR analysis of raw CYP, PPy, CYP–PPy composite, and CYP–PPy after CR adsorption. The broad peak at 3200–3600 cm^{-1} can be attributed to hydroxyl group stretching vibration from CYP. In the CYP, the peak at 2925 cm^{-1} corresponds to the C–H asymmetrically stretching vibration. The peak near 1642 cm^{-1} and 1545 cm^{-1} might be endorsed to the stretching vibration of C=C. The band appeared at 1029 cm^{-1} indicates the N–H stretching. The sharp peak at 1541 cm^{-1} in PPy represents the C=C stretching of pyrrole ring.[3,26] The band at 1457 cm^{-1} might be assigned to the symmetric pyrrole ring stretching and conjugated C–N stretching.[11,27] Peaks at 1166 cm^{-1} and 1038 cm^{-1} are assigned to the C–H and N–H in-plane deformation vibration, respectively. And the band of C–H out-plane vibration is observed at 898 cm^{-1}. These characteristic peaks accompanying with PPy also existed in CYP–PPy composite, and the peak of 1541 cm^{-1} assigned to pyrrole ring is enhanced in CYP–PPy, thus evidently confirming the successful introduction of PPy to CYP. The spectrum of CYP–PPy after CR adsorption was also presented. After the CYP–PPy loaded with CR, shifting of peaks of CYP–PPy from 2925, 1541, 1457, 1166, 1038, and 898 cm^{-1} to 2930, 1554, 1462, 1175, 1046, and 910 cm^{-1} was observed. It seems that these respective functional groups most likely to be involved in dye interaction during the adsorption. XRD patterns of raw CYP, PPy and CYP–PPy were shown in Fig. 3b. The peaks at 14.47° and 22.14° are related to the presence of cellulose in CYP, and the broad peak of 22.14° denotes the natural amorphous structure of CYP. For the XRD pattern of PPy, the manifest peak at 23.12° is observed, implying an amorphous nature. The result is consistent with the reported literature. The spectra for CYP–PPy showed this characteristic peak is fused into CYP.[20]

Fig. 4 shows the TGA curves of CYP, PPy, CYP–PPy composite. The TGA curve of CYP indicated the thermal degradation occurs up to 200 °C with a weight loss of about 17%. This may be accounted to the loss of moisture. Then, a continuous loss of approximately 56% was observed in the temperature range of 200–500 °C. This major mass loss is due to

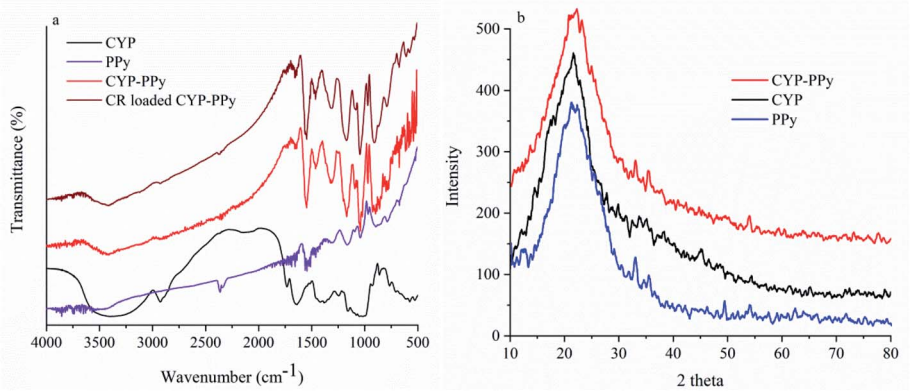

Fig. 3 (a) FTIR (CYP, PPy, CYP–PPy and CYP–PPy after adsorption) and (b) XRD analysis of CYP, PPy, and CYP–PPy.

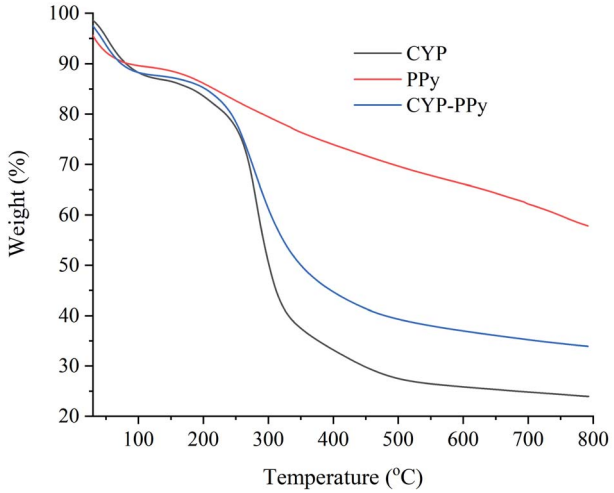

Fig. 4 TGA curves of CYP, PPy and CYP–PPy.

the decomposition of biomass matter. However, the thermal stability of CYP–PPy composite was discovered to be relatively improved, which may be owing to the higher thermal stability of PPy.[3] Finally, the weight losses of CYP and CYP–PPy composite were estimated to be approximately 76% and 66% at the end of the analysis, at 800 °C, respectively. The nitrogen adsorption–desorption isotherms of CYP and CYP–PPy are illustrated in Fig. 5. The BET surface area of CYP–PPy is found to be 79.955 m^2 g^{-1}, which is much higher than that of CYP of 16.548 m^2 g^{-1}. The greater specific surface area of CYP–PPy offers more binding sites for adsorption. The result indicates that introducing PPy to CYP can improve the surface feature of the adsorbent (Table 1).

3.2 Comparison of CYP and CYP–PPy

Chinese yam peel is a low-cost bio-source adsorbent. As an agricultural waste, it can be a fine material for dye removal. In the CYP–PPy, polypyrrole particles with diffused morphology dispersed on the surface of CYP particles, which increases the

Table 1 Surface area, pore volume and pore diameter for CYP and CYP–PPy

Parameter	CYP	CYP–PPy
Surface area (S_{BET}) (m^2 g^{-1})	16.548	79.955
Pore volume (V_p) (cm^3 g^{-1})	0.017	0.094
Pore diameter (d_p) (nm)	2.107	2.574

removal efficiency of the CYP–PPy composite. Although the removal efficiency of the CYP–PPy is relatively lower than that of PPy, it is fair to indicate that the prepared CYP–PPy was a promising material to remove CR from aqueous solution. The adsorption data were provided in Table 2 to justify the successful modification of Chinese yam peel.

3.3 Effect of adsorbent dosage

Adsorbent dosage is a significant parameter in the dye removal process. The quantitative performance of CYP–PPy composite for the removal of CR dye from aqueous media was assessed by varying adsorbent dosage from 0.8 to 12 g L^{-1}, and the results are manifested graphically in Fig. 6. According to Fig. 6, the adsorbent exhibits a remarkable increasing the removal efficiency of CR from 70.73% to 99.50% in the range of investigation dosage. This enhancement can be attributed to the more available active sites and greater adsorbing surface area for adsorption at higher adsorbent dosage. Meantime, the lower adsorption capacity was observed with increasing amount of adsorbent. Numerically, the adsorption capacity of CYP–PPy composite decreased from 88.41 to 8.29 mg g^{-1}. The downtrend in the adsorption capacity may be due to the decreasing of vacant adsorbing sites per unit mass of adsorbent owing to the agglomeration at higher dosage.[3] In fact, considering the removal efficiency and adsorption capacity, the CYP–PPy composite dosage of 10 g L^{-1} was opted for the following tests.

3.4 Effect of pH

The solution pH has an important effect on dye removal by changing the surface property of adsorbent material and

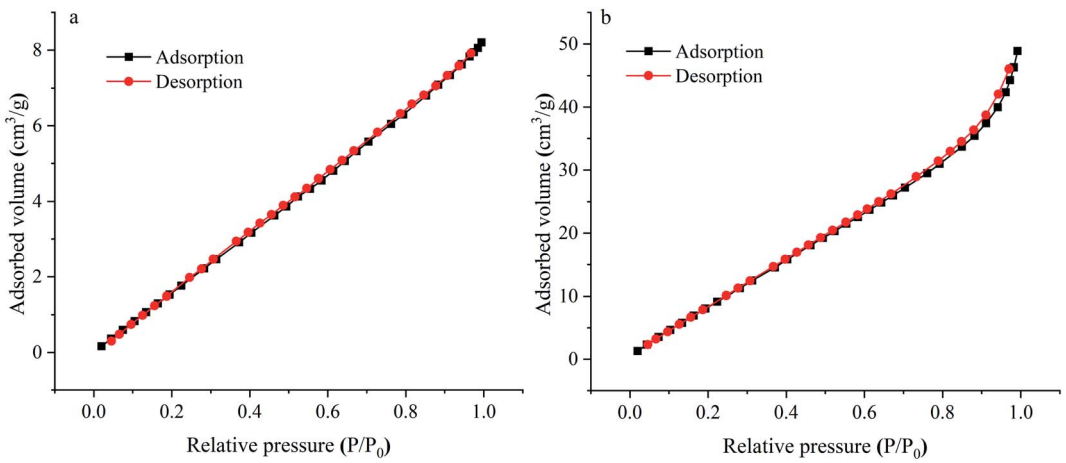

Fig. 5 Nitrogen adsorption–desorption isotherm of CYP (a) and CYP–PPy (b).

Table 2 Adsorption efficiency of CYP, PPy and CYP–PPy in CR removal at equilibrium time

No.	Adsorbent	Adsorbent dose (g L^{-1})	Initial CR concentration (mg L^{-1})	Removal efficiency (%)
1	CYP	2	100	46.61
2	PPy	2	100	87.29
3	CYP–PPy	2	100	77.99

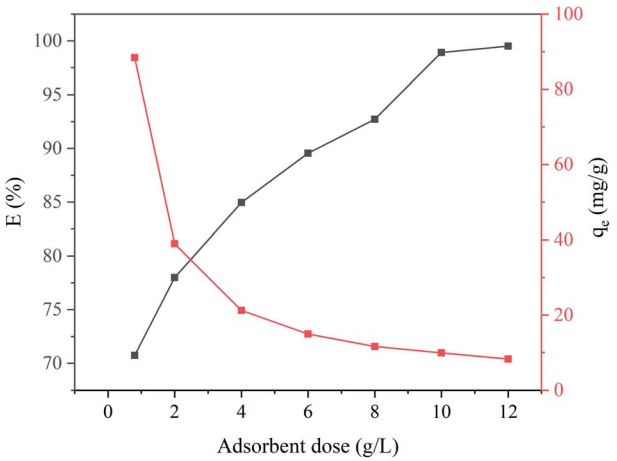

Fig. 6 Effect of adsorbent dose on CR adsorption.

adsorbent–adsorbate interactions. The efficiency of CYP–PPy composite for CR removal was tested with a pH range of 4 to 11. The obtained results are shown in Fig. 7. In general, a higher CR removal is achieved under acidic condition. A possible explanation may be due to the positive surface charge of CYP–PPy at acidic pH. Then, the negative electric charge of CR shows affinity towards CYP–PPy by electrostatic attraction. Derouich *et al.* also reported that an acidic condition is suitable for anionic dye adsorption.[2]

3.5 Time effect and adsorption kinetics

The effect of absorbing time on adsorption performance of CYP–PPy composite is given in Fig. 8a and b. It is clear that the

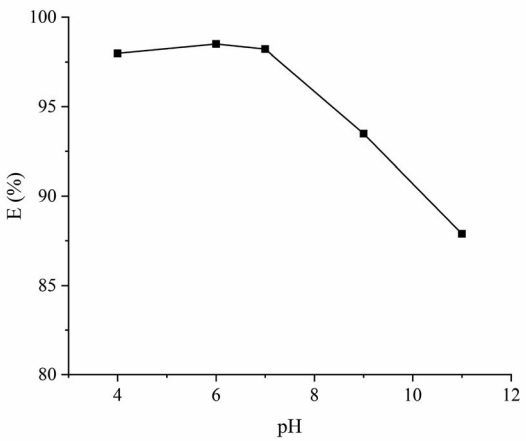

Fig. 7 Effect of pH for CR removal.

removal efficiency increases initially at a highly rapid rate because a great many available surface-active sites will be occupied gradually over the time. Until 60 min, the removal efficiency reached 74.35% at the initial concentration of 100 mg L^{-1}. Then, the removal of CR was slowed down with the prolongation of time owing to the decrease in adsorption capacity. This declining trend is attributed to the decline in active-sites, as well as the deeper and farther transfer of adsorbate molecules.[3] In the final stage (300–400 min), the equilibrium was established. It is much clear that the adsorption capacity increases with the increasing of the CR initial concentration. The concentration gradient plays the role of driving force for the transfer process.[26]

The adsorption kinetics of CR on CYP–PPy composite was studied under different initial concentrations in detail. To understand the deeper mechanism of adsorption process, the experimental data were analyzed with various kinetic models including pseudo-first-order, pseudo-second-order, Elovich, and intra-particle diffusion. The models are represented in Text S1.† The fitting results are listed in Table 3 and the adsorption process of CR on CYP–PPy composite follows the pseudo-second-order kinetic model (Fig. 8c). The calculated values of q_e by the pseudo-second-order kinetic model are much closer to the values determined *via* experiment. The result indicates that chemisorption is the limited step in the adsorption of CR on the surface of material.[28] The chemical adsorption process involves electron sharing or transfer between CR (adsorbate) and CYP–PPy composite (adsorbent). In addition, the corresponding constant k_2 value is inversely proportional to the initial concentration of CR, which means the lower initial concentration of CR declines the adsorption rate.[26] Also, the relatively high value of R^2 in pseudo-first-order model could not be ignored, which indicates some area of the adsorbent is occupied physically. Hence, the adsorption process may be a combination of chemical-physical procedure. The similar result was also reported by Khadir *et al.*[11] Meanwhile, the relatively high value of R^2 in Elovich model (0.9554–0.9958) suggests that the adsorption behavior is not only chemisorption. In spite of the comparison with former kinetic models, pseudo-second-order model is still more favorable. It can still reveal that the adsorbent sites are not heterogeneous. The above mentioned findings demonstrate that the adsorption of CR onto CYP–PPy involves more than one mechanism.

To obtain more insight into the comprehensive mechanism of adsorption of CR onto CYP–PPy composite, intra-particle diffusion model was also applied to evaluate stages of adsorption process. The result is shown in Fig. 8d. It can be seen that the adsorption process of CR on CYP–PPy composite has

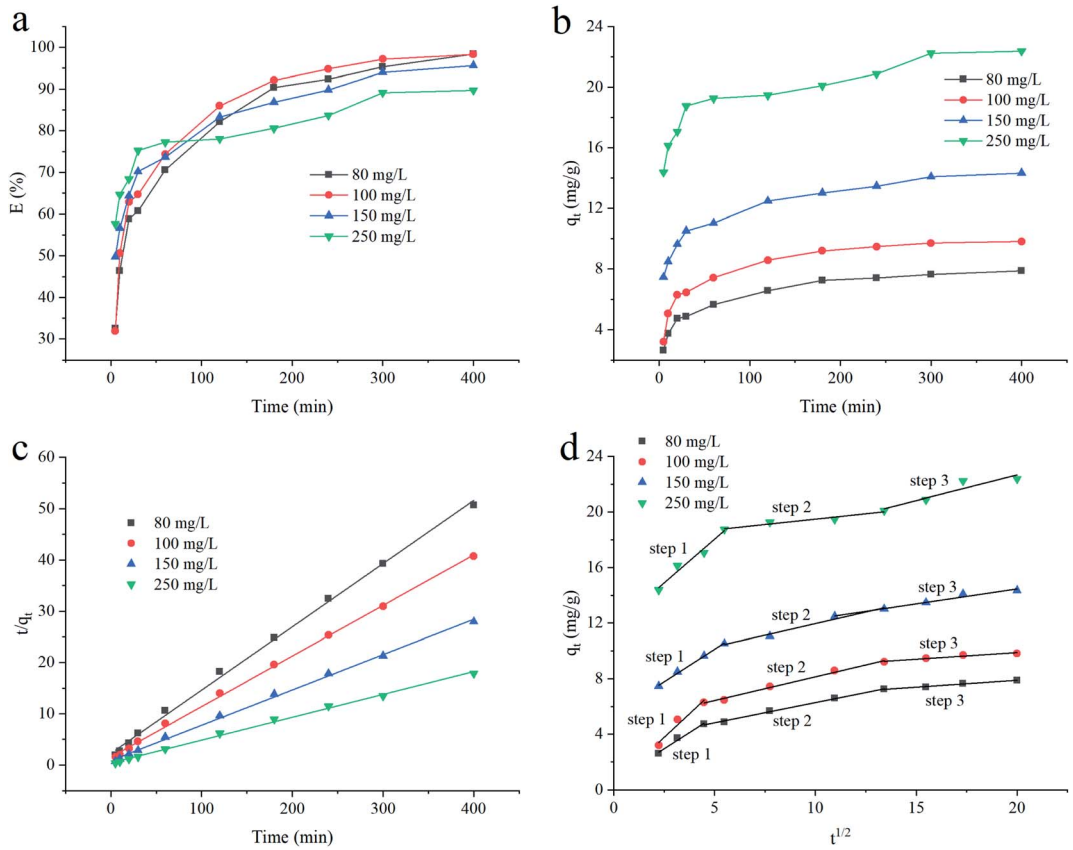

Fig. 8 Effect of time on CR adsorption (a and b), pseudo-second-order kinetic model (c) and intraparticle diffusion model (d) for adsorption of CR onto CYP–PPy composite.

Table 3 Kinetic parameters for the adsorption of CR onto CYP–PPy composite

C_0 (mg L^{-1})	80	100	150	250
Pseudo-first-order				
$q_{e,cal}$	4.3970	5.2972	6.0466	7.0460
k_1	3.81×10^{-3}	4.93×10^{-3}	3.00×10^{-3}	3.48×10^{-3}
R^2	0.9869	0.9931	0.9822	0.9202
Pseudo-second-order				
$q_{e,cal}$	8.1031	10.1338	14.5117	22.4014
k_2	6.73×10^{-3}	6.40×10^{-3}	5.48×10^{-3}	5.08×10^{-3}
R^2	0.9980	0.9991	0.9979	0.9972
Elovich				
α	2.5286	3.9225	35.6654	2505.5764
β	0.8421	0.6837	0.6356	0.6020
R^2	0.9939	0.9814	0.9958	0.9554
Intra-particle diffusion				
Step 1: k_p	0.9289	1.3543	0.9342	1.2609
C	0.6264	0.3853	5.4405	11.7416
R^2	0.9830	0.9529	0.9970	0.9687
Step 2: k_p	0.2911	0.3420	0.3332	0.1546
C	3.3640	4.7155	8.6277	17.9431
R^2	0.9972	0.9927	0.9801	0.9440
Step 3: k_p	0.1000	0.0957	0.2154	0.3677
C	5.8881	7.9680	10.1465	15.3028
R^2	0.9928	0.9417	0.9746	0.8821

multiple diffusion steps. Namely, the first stage represents the fast diffusion of adsorbate target (CR) through solution to the surface of adsorbent particles. In the second and the third stages, the rate of adsorption gradually slows down. These imply the diffusion of adsorbate into the inner pores of adsorbent particles, thus the increased diffusion resistance leading to the balanced state. Since lines do not pass through the origin, the intra-granular diffusion is not the only controlling step, but also involving other adsorption process.

3.6 Initial concentration and adsorption isotherms

The research of adsorption isotherms is necessary. Herein, the study was conducted at different temperatures in a wide initial dye concentrations range (80–1000 mg L^{-1}). The isotherm data were studied with various isothermal models including Langmuir, Freundlich, D–R, and Temkin. The linearization equations of above-mentioned models are given in Text S2.† All the corresponding parameters obtained are shown in Table 4. As shown in the Table 4, the higher values of R^2 in the Langmuir model suggest that the adsorption of dye molecules on the CYP–PPy composite is monolayer adsorption. And the fitting result is displayed in Fig. 9b. The values of q_m are closely consistent with obtained experimental data. The increasing trend of q_m with the rise of adsorption temperature indicates that the increasing of temperature is favorable for dye removal, which implies that the

Table 4 Parameters of isotherm models for CR onto CYP–PPy composite

Temperature (°C)	15	25	35	45
Langmuir				
q_m	53.1632	59.8086	82.6446	86.6551
K_l	0.0560	0.0800	0.1673	0.5377
R^2	0.9943	0.9914	0.9913	0.9961
R_L	0.0249–0.1824	0.0175–0.1352	0.0059–0.0695	0.0019–0.0227
Freundlich				
n	2.4840	2.7364	3.7776	3.7477
K_f	6.5267	10.0648	20.1829	27.1137
R^2	0.9512	0.9864	0.9744	0.9155
D–R				
K_D	1.88×10^{-6}	3.07×10^{-7}	2.47×10^{-8}	2.53×10^{-8}
q_m	29.5664	30.9561	38.8376	48.8815
R^2	0.7157	0.6790	0.6476	0.7941
Temkin				
A_T	0.8841	2.5661	31.5672	64.4319
b_T	260.4260	278.6422	323.7850	298.6917
R^2	0.9651	0.9482	0.8874	0.9551

adsorption process is endothermic (Section 3.7). Further, the values of dimensionless separation factor (R_L) in the study are in the range of 0.0019–0.1824, which clearly indicates that the adsorption process was favorable ($0 < R_L < 1$). However, the relatively high R^2 values in Freundlich isotherm suggest that multilayer adsorption also plays a crucial role in CR uptake. It implies that the CYP–PPy composites act like heterogeneous media for CR molecule. The values of $1/n$ in this study lie between 0.2647 to 0.4026 at investigated temperature, indicating that CR removal was favorable (since $0 < 1/n < 0.5$).[11] So, the chemisorption is also non-ignored. In conclusion, the adsorption of CR on CYP–PPy composite can be defined as a mixture process. Namely, physical and chemical adsorption control the removal process.

3.7 Thermodynamic studies

The thermodynamic parameters for CR are presented in Table 5. The negative values of ΔG suggested the spontaneity of the adsorption system. It is seen that a higher absolute value of ΔG was observed at greater temperature. Thus, the adsorption process is more spontaneous and favorable at higher temperature. Positive ΔH suggested that the process is endothermic, which reflects that higher temperatures are more satisfactory for CR adsorption onto CYP–PPy. The result is consistent with the previous experimental results. Generally speaking, enthalpy value greater than 40 kJ mol^{-1} reveals a chemisorption.[11] Herein, ΔH was found to be 81.6691 kJ mol^{-1}, which indicating

Table 5 Thermodynamic parameters of CR adsorption onto CYP–PPy

Temperature (K)	ΔG (kJ mol^{-1})	ΔH (kJ mol^{-1})	ΔS (kJ mol^{-1} K^{-1})
288	−1.6475	81.6691	0.2876
298	−2.9595		
308	−7.5224		
318	−9.7572		

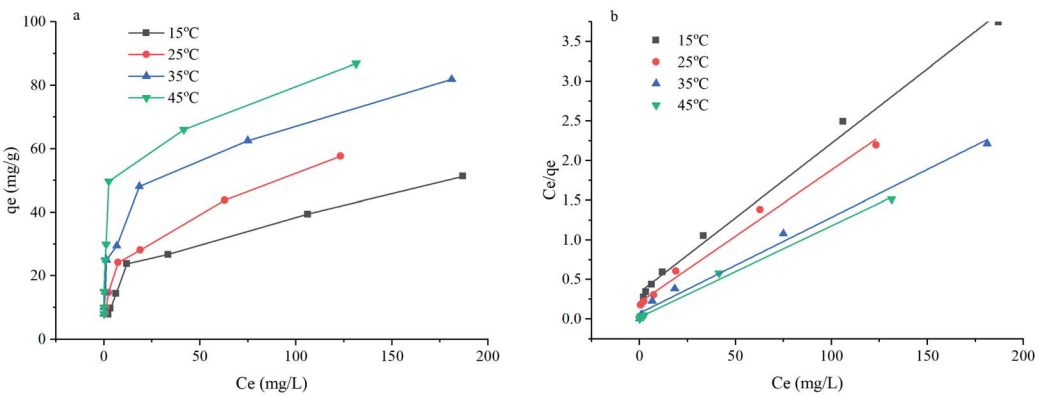

Fig. 9 Adsorption isotherms at different temperatures (a), and the Langmuir isotherm model for CR (b).

Table 6 Comparison the adsorption capacity of CYP–PPy with other adsorbents for dye removal

No.	Adsorbent	Dye	Adsorption capacity ($mg\ g^{-1}$)	Ref.
1	m-Cell/Fe_3O_4/ACCs	Congo red	66.09	5
2	Activated carbon	Congo red	6.70	29
3	AAK/TiO_2-30	Congo red	38.70	30
4	*p*TSA-Pani@GO–CNT	Congo red	66.66	32
5	Cr_2O_3/Al_2O_3	Congo red	35.13	33
6	PPy/MW nanocomposite	Congo red	147.00	31
7	Polypyrrole/starch	Acid Black-234	66.6	1
8	Sisal fibers/polypyrrole/polyaniline	Reactive orange 5	12.43	11
9	MChs/Ppy	Crystal violet	62.89	3
10	CYP–PPy	Congo red	86.66	This work

that chemisorption mechanism of CR molecules onto CYP–PPy is existing. Also, positive ΔS suggests an increase in disorder and randomness at the solution/solid interface. Hence, the change of entropy reveals good affinity of the obtained adsorbent for adsorbate.

3.8 Comparison with other relevant work

To evaluate the applicability of CYP–PPy, we compare the performance of CYP–PPy in this work with other adsorbents in terms of adsorption capacity. The result was exhibited in Table 6. According to the data, it can be suggested that CYP–PPy is successful for dye removal in comparison with other adsorbents such as m-Cell/Fe_3O_4/ACCs,[5] activated carbon,[29] AAK/TiO_2-30,[30] sisal fibers/polypyrrole/polyaniline.[11] However, it is relatively inferior to the adsorbent of PPy/MW nanocomposite.[33] All the same, it is obvious that CYP–PPy has competitive adsorption capacity compared to the adsorbents in the table. It can be concluded that the CYP–PPy proposed in this work can be successfully utilized for dye wastewater treatment.

3.9 Mechanism of adsorption

In order to understand the interaction mechanism involved in the adsorption process, it is necessary to consider the surface nature of CYP–PPy and the structure of CR dye. The schematic illustration of proposed mechanism is illustrated in Fig. 10. The CR molecules are primarily adsorbed by pH-dependent electrostatic attraction and π–π interaction. Under acidic medium, protonated amine groups of CYP–PPy composite bring about positive surface charge. Fortunately, CR is a kind of anionic dye having sodium sulfonate groups, which can dissociate sulfonate group owing negative charge. Thus, electrostatic attraction between the protonated amine groups and sulfonate groups might be the main mechanism for the adsorption process. A similar mechanism was also proposed in the previous reported literature. Electrostatic interaction can be consider as the primary mechanism for the adsorption process, but is not the only interaction mechanism. The other interaction forces like π–π interaction and H-bonding can also play essential role in the adsorption process.

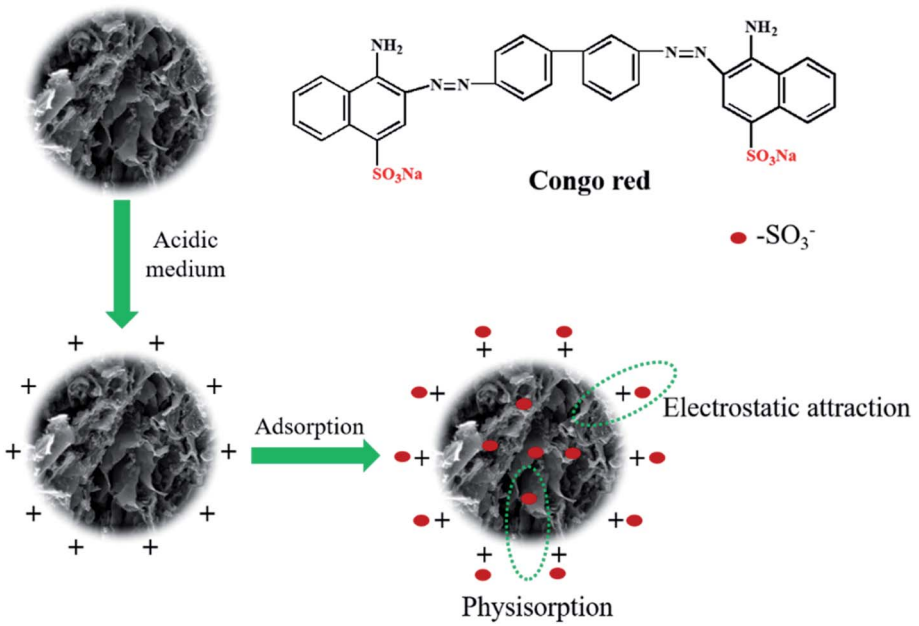

Fig. 10 Schematic illustration of proposed mechanism for CR removal by CYP–PPy.

3.10 Reusability study

In this study, desorption tests were conducted with different desorbing solvents. The results indicate that a higher desorption efficiency of CR from dye-loaded-CYP–PPy adsorbent resulted in 0.1 M NaOH. Moreover, the adsorbent was executed with 0.1 M NaOH for three successive cycles of ad-/de-sorption. According the results displayed in Fig. S2,† the removal efficiency was dropped to 94.8% in the third usage stage. However, it was declined to 84.6% in the fourth time. Therefore, the result represented that CYP–PPy is stable to be employed for the high removal of CR dye.

4. Conclusions

The potential of CYP–PPy as a low-cost, nontoxicity, and availability adsorbent for removal of CR was evaluated in the present research. Herein, *in situ* polymerization technique was efficacious for modifying Chinese yam peel with polypyrrole. The result was confirmed by FTIR, SEM, TEM, XRD, and TG. The variables including adsorbent dosage, pH of the system, contacting time, initial concentration, and adsorption temperature have significant effect on the removal efficiency of CR. The equilibrium removal efficiency reached 98.9% at the adsorbent dosage of 10 g L^{-1}, and the initial concentration of 100 mg L^{-1}. The adsorption equilibrium data manifested the applicability of Langmuir isotherm model for CR removal with the maximum adsorption capacity of 86.66 mg g^{-1} at 45 °C. Langmuir and pseudo-second-order models could give a satisfactory explain explanation that the adsorption process was endothermic and chemisorption. The main mechanism for the CR removal was deemed as electrostatic interaction. But, pseudo-first-order model could not be ignored, and the CR removal was also governed by intra-particle diffusion. So, the adsorption process was a combination of chemical-physical procedure. Maximum desorption of CR form dye loaded-CYP–PPy was obtained with 0.1 M NaOH, and the adsorbent was reused effectively up to three successive cycles of ad-/de-sorption. Hence, CYP–PPy is perspective to be employed for dye pollution control. This work provides an alternative scheme for the targeted exploitation of agricultural waste.

Conflicts of interest

The authors declare that they have no any commercial or associative interest that could influence the work reported in this submitted paper.

Acknowledgements

This work was supported by the University Natural Science Research Project of Anhui Province (No. KJ2021A0884) and the Project of Anhui Science and Technology University for Talent Introduction (No. SKYJ201601). The work also acknowledges the support from the National College Student Innovation Training Program (No. 202010879).

References

1 S. Noreen, H. N. Bhatti, M. Iqbal, F. Hussain and F. M. Sarim, Chitosan, starch, polyaniline and polypyrrole biocomposite with sugarcane bagasse for the efficient removal of Acid Black dye, *Int. J. Biol. Macromol.*, 2020, **147**, 439–452.

2 G. Derouich, S. A. Younssi, J. Bennazha, J. A. Cody, M. Ouammou and M. El Rhazi, Development of low-cost polypyrrole/sintered pozzolan ultrafiltration membrane and its highly efficient performance for congo red dye removal, *J. Environ. Chem. Eng.*, 2020, **8**(3), 103809.

3 F. Mashkoor and A. Nasar, Facile synthesis of polypyrrole decorated chitosan-based magsorbent: Characterizations, performance, and applications in removing cationic and anionic dyes from aqueous medium, *Int. J. Biol. Macromol.*, 2020, **161**, 88–100.

4 Y. Wang, L. Qian, Y. Miao, Y. Zhao, R. Li and J. Tang, Ionic liquid pretreatment as an emerging approach for synthesis of a magnetic adsorbent derived from Broussonetia papyrifera leaves for dye removal, *Sep. Sci. Technol.*, 2018, **54**(18), 3019–3026.

5 H. Y. Zhu, Y. Q. Fu, R. Jiang, J. H. Jiang, L. Xiao, G. M. Zeng, S. L. Zhao and Y. Wang, Adsorption removal of congo red onto magnetic cellulose/Fe3O4/activated carbon composite: Equilibrium, kinetic and thermodynamic studies, *Chem. Eng. J.*, 2011, **173**(2), 494–502.

6 D. A. González-Casamachin, J. Rivera De la Rosa, C. J. Lucio-Ortiz, D. A. De Haro De Rio, D. X. Martínez-Vargas, G. A. Flores-Escamilla, N. E. Dávila Guzman, V. M. Ovando-Medina and E. Moctezuma-Velazquez, Visible-light photocatalytic degradation of acid violet 7 dye in a continuous annular reactor using ZnO/PPy photocatalyst: Synthesis, characterization, mass transfer effect evaluation and kinetic analysis, *Chem. Eng. J.*, 2019, **373**, 325–337.

7 T. Shahnaz, S. M. M. Fazil, V. C. Padmanaban and S. Narayanasamy, Surface modification of nanocellulose using polypyrrole for the adsorptive removal of Congo red dye and chromium in binary mixture, *Int. J. Biol. Macromol.*, 2020, **151**, 322–332.

8 V. Arumugam, P. Sriram, T. J. Yen, G. G. Redhi and R. M. Gengan, Nano-material as an excellent catalyst for reducing a series of nitroanilines and dyes: triphosphonated ionic liquid- CuFe2O4-modified boron nitride, *Appl. Catal., B*, 2018, **222**, 99–114.

9 H. Yang, L. Bai, D. Wei, L. Yang, W. Wang, H. Chen, Y. Niu and Z. Xue, Ionic self-assembly of poly(ionic liquid)-polyoxometalate hybrids for selective adsorption of anionic dyes, *Chem. Eng. J.*, 2019, **358**, 850–859.

10 M. Tanzifi, M. T. Yaraki, Z. Beiramzadeh, L. H. Saremi, M. Najafifard, H. Moradi, M. Mansouri, M. Karami and H. Bazgir, Carboxymethyl cellulose improved adsorption capacity of polypyrrole/CMC composite nanoparticles for removal of reactive dyes: Experimental optimization and DFT calculation, *Chemosphere*, 2020, **255**, 127052.

11 A. Khadir, M. Negarestani and H. Ghiasinejad, Low-cost sisal fibers/polypyrrole/polyaniline biosorbent for sequestration

of reactive orange 5 from aqueous solutions, *J. Environ. Chem. Eng.*, 2020, **8**(4), 103956.

12 M. K. Purkait, A. Maiti, S. DasGupta and S. De, Removal of congo red using activated carbon and its regeneration, *J. Hazard. Mater.*, 2007, **145**(1–2), 287–295.

13 H. D. da Rocha, E. S. Reis, G. P. Ratkovski, R. J. da Silva, F. D. S. Gorza, G. C. Pedro and C. P. de Melo, Use of PMMA/(rice husk ash)/polypyrrole membranes for the removal of dyes and heavy metal ions, *J. Taiwan Inst. Chem. Eng.*, 2020, **110**, 8–20.

14 L. Yang, M. Lv, Y. Song, K. Yin, X. Wang, X. Cheng, K. Cao, S. Li, C. Wang, Y. Yao, W. Luo and Z. Zou, Porous Sn3O4 nanosheets on PPy hollow rod with photo-induced electrons oriented migration for enhanced visible-light hydrogen production, *Appl. Catal., B*, 2020, **279**, 119341.

15 S. Nag, A. Ghosh, D. Das, A. Mondal and S. Mukherjee, Ni0.5Zn0.5Fe2O4/polypyrrole nanocomposite: A novel magnetic photocatalyst for degradation of organic dyes, *Synth. Met.*, 2020, **267**, 116459.

16 B. C. Pires, T. A. do Nascimento, F. V. A. Dutra and K. B. Borges, Removal of a non-steroidal anti-inflammatory by adsorption on polypyrrole/multiwalled carbon nanotube composite—Study of kinetics and equilibrium in aqueous medium, *Colloids Surf., A*, 2019, **578**, 123583.

17 X. Yang, Y. Mi, F. Liu, J. Li, H. Gao, S. Zhang, W. Zhou and R. Lu, Preparation of magnetic attapulgite/polypyrrole nanocomposites for magnetic effervescence-assisted dispersive solid-phase extraction of pyrethroids from honey samples, *J. Sep. Sci.*, 2020, **43**(12), 2419–2428.

18 W. Yan, X. Wan, Y. Xu, X. Lv and Y. Chen, A phenalenyl-based neutral stable π-conjugated polyradical, *Synth. Met.*, 2009, **159**(17–18), 1772–1777.

19 M. Bhaumik, R. McCrindle and A. Maity, Efficient removal of Congo red from aqueous solutions by adsorption onto interconnected polypyrrole-polyaniline nanofibres, *Chem. Eng. J.*, 2013, **228**, 506–515.

20 S. Rafiaee, M. R. Samani and D. Toghraie, Removal of hexavalent chromium from aqueous media using pomegranate peels modified by polymeric coatings: Effects of various composite synthesis parameters, *Synth. Met.*, 2020, **265**, 116416.

21 S. Kamal, F. Khan, H. Kausar, M. S. Khan, A. Ahmad, S. I. Ahmad, M. Asim, W. Alshitari and S. A. A. Nami, Synthesis, characterization, morphology, and adsorption studies of ternary nanocomposite comprising graphene oxide, chitosan, and polypyrrole, *Polym. Compos.*, 2020, **41**(9), 3758–3767.

22 I. Anastopoulos and G. Z. Kyzas, Agricultural peels for dye adsorption: A review of recent literature, *J. Mol. Liq.*, 2014, **200**, 381–389.

23 U. Herrera-García, J. Castillo, D. Patiño-Ruiz, R. Solano and A. Herrera, Activated Carbon from Yam Peels Modified with Fe3O4 for Removal of 2,4-Dichlorophenoxyacetic Acid in Aqueous Solution, *Water*, 2019, **11**, 2342.

24 Y. F. Huang, J. H. Peng and X. J. Huang, One-pot preparation of magnetic carbon adsorbent derived from pomelo peel for magnetic solid-phase extraction of pollutants in environmental waters, *J. Chromatogr. A*, 2018, **1546**, 28–35.

25 H. Y. Xue, J. R. Li, Y. G. Liu, Q. Gao, X. W. Wang, J. W. Zhang, M. Tanokura and Y. L. Xue, Optimization of the ultrafiltration-assisted extraction of Chinese yam polysaccharide using response surface methodology and its biological activity, *Int. J. Biol. Macromol.*, 2019, **121**, 1186–1193.

26 Z. Chen and K. Pan, Enhanced removal of Cr(VI) *via in situ* synergistic reduction and fixation by polypyrrole/sugarcane bagasse composites, *Chemosphere*, 2021, **272**, 129606.

27 J. Y. Hong, H. Yoon and J. Jang, Kinetic study of the formation of polypyrrole nanoparticles in water-soluble polymer/metal cation systems: a light-scattering analysis, *Small*, 2010, **6**(5), 679–686.

28 H. Ma, J. B. Li, W. W. Liu, M. Miao, B. J. Cheng and S. W. Zhu, Novel synthesis of a versatile magnetic adsorbent derived from corncob for dye removal, *Bioresour. Technol.*, 2015, **190**, 13–20.

29 C. Namasivayam and D. Kavitha, Removal of Congo Red from water by adsorption onto activated carbon prepared from coir pith, an agricultural solid waste, *Dyes Pigm.*, 2002, **54**(1), 47–58.

30 Y. Hai, X. Li, H. Wu, S. Zhao, W. Deligeer and S. Asuha, Modification of acid-activated kaolinite with TiO_2 and its use for the removal of azo dyes, *Appl. Clay Sci.*, 2015, **114**, 558–567.

31 R. S. Aliabadi and N. O. Mahmoodi, Synthesis and characterization of polypyrrole, polyaniline nanoparticles and their nanocomposite for removal of azo dyes; sunset yellow and Congo red, *J. Cleaner Prod.*, 2018, **179**, 235–245.

32 M. O. Ansari, R. Kumar, S. A. Ansari, S. P. Ansari, M. A. Barakat, A. Alshahrie and M. H. Cho, Anion selective pTSA doped polyaniline@graphene oxide-multiwalled carbon nanotube composite for Cr(VI) and Congo red adsorption, *J. Colloid Interface Sci.*, 2017, **496**, 407–415.

33 M. M. Ibrahim, Cr2O3/Al2O3 as adsorbent: Physicochemical properties and adsorption behaviors towards removal of Congo red dye from water, *J. Environ. Chem. Eng.*, 2019, **7**(1), 102848.